Modeling and Control of an Islanded Campus Microgrid with Coordinated CHP and PV Systems

Jimiao Zhang, *Student Member, IEEE,* and Jie Li, *Member, IEEE*
Electrical and Computer Engineering, Rowan University, Glassboro, NJ, USA (zhangj52.students, lijie@rowan.edu)

***Abstract*—On-site power generation systems, integrating combined heat and power (CHP) and solar photovoltaics (PVs), could bring significant energy cost savings to the electricity consumers and reduce carbon emissions. This paper presents detailed modeling of an existing gas-turbine-based 5-MVA CHP unit located on a university campus. In addition, integration of a 10-MW solar farm into the campus microgrid is investigated. A virtual synchronous generator (VSG) approach is proposed to control the PV system as a double-stage PV-VSG, which emulates the rotational inertia of a conventional synchronous generator (SG) using only the dc-link capacitor. The coordinated control of the two generation facilities is studied when the microgrid is in islanded mode. The large capacity of the PV farm is leveraged to serve part of the campus baseload demand when sufficient solar power is available, while the CHP is on hot standby. When the grid frequency stabilizes, the CHP will be brought online for load sharing. The underfrequency load shedding (UFLS) is also in place to arrest the potential rapid frequency fall. The simulated campus microgrid system is developed in MATLAB/Simulink to verify the modeling accuracy and control performance.**

***Index Terms*—Combined heat and power (CHP), photovoltaic (PV), virtual synchronous generator, droop control, microgrid.**

I. Introduction

Microgrids are small self-sufficient power systems that can operate independently of the utility grid, i.e., in islanded mode. Their infrastructure facilitates the ever-increasing deployment of distributed energy resources (DERs) to achieve resiliency, economy, and sustainability goals. Among the mix of DER fleet, the combined heat and power (CHP) and the solar photovoltaics (PVs) are two technologies that have been gaining traction worldwide.

CHP, also known as cogeneration, is often extolled for its high energy conversion efficiency by harnessing the waste heat produced during the electricity generation process. The collected heat is used for heating or cooling buildings, or for some heat-intensive industrial processes. Moreover, CHP generally consumes greener fuels such as natural gas, biomass, or biogas with reduced carbon emissions. In an islanded microgrid, CHP could be base-loaded or used as spinning reserve to overcome intermittency of renewable energy sources (RESs). A CHP unit mainly consists of a prime mover (e.g., a gas turbine (GT) or fuel cells), a generator, and a heat recovery system. Modeling of CHP units has long been an ongoing research topic, and there have been several types of models [1-3] in the literature. However, the Rowen's model, which was initially developed for industrial heavy-duty GTs, is well recognized as more explicit in terms of control functions [4] than the others.

Conventionally, the grid integration of PV systems is based on grid-following inverters to take advantage of the free RES in the maximum power point (MPP) tracking mode. However, grid-following inverters are unable to help regulate the system voltage or frequency [5]. As the penetration of inverter based RESs continues to increase, low-inertia power grids are experiencing greater frequency excursions and voltage variations [5] due to decreased inertia and reactive power support from synchronous generators (SGs). To date, some efforts have been directed towards controlling the PV systems as virtual SGs (VSGs) with improved damping and inertia. Intrinsically, these VSGs are built upon grid-supporting inverters with droop control. In the literature, there are primarily two types of PV-VSG approaches. In some studies, energy storage systems (ESSs) and their bi-directional dc-dc converters are placed at the dc link to stabilize the voltage [6-7]. Obviously, the ESSs would incur additional costs. In addition, the contribution of PV cannot be explicitly justified because the primary regulation is only provided by the ESSs. Other methods eliminate ESSs, and PV-VSGs are controlled away from the MPP to provide active power reserve [8-9] or using the dc-link capacitor of the inverter to provide inertia support [10-11]. However, a phase-locked loop (PLL) is required in [8, 9, 11], which might cause instability issues, particularly in a non-stiff grid. Further, some papers such as [8] adopt a single stage topology, thus limiting the PV operating range. To this end, addition of a dc-dc stage is preferred. The proposed PV-VSGs in [10-11] were validated only in a single-DER system. And the effect of solar irradiance (SI) on the PV-VSG operation was not investigated in [10]. As solar power shortage is possible, control of a PV-VSG without ESSs needs to be coordinated with other DERs in islanded microgrids.

The main contributions of this work are:

1) A double-stage PV-VSG model is proposed to model the 10-MW PV farm in a campus microgrid. This configuration does not necessitate ESSs or PLLs. In addition, a single-shaft GT is accurately modeled to simulate the Solar Centaur 40 CHP unit located on the university campus.

978-1-6654-0507-2/21/$31.00 ©2021 IEEE

Authorized licensed use limited to: Stevens Institute of Technology. Downloaded on February 12,2022 at 16:15:33 UTC from IEEE Xplore. Restrictions apply.

2) Coordinated control between the PV farm and the CHP unit under SI intermittency with underfrequency load shedding (UFLS) in place is studied for the stable operation of the campus microgrid in islanded mode.

The remainder of this paper is organized as follows: Section II presents the detailed modeling of the single-shaft GT-based CHP unit. Section III discusses the modeling and control of the double-stage PV-VSG system. Numerical simulation results of coordinated control between the two systems in the campus microgrid are presented in Section IV. Section V concludes this paper and discusses the future work.

II. CHP Modeling

Fig. 1 shows a typical single-shaft GT-based CHP unit with its major components [2]: a compressor, a combustor, and an expansion turbine (ET). The heated flow expanded in the ET drives the compressor and the generator (G), while the heat recovery steam generator (HRSG) recovers waste heat from the exhaust gases. The steam produced by the HRSG can be used for heating/cooling or to drive a steam turbine.

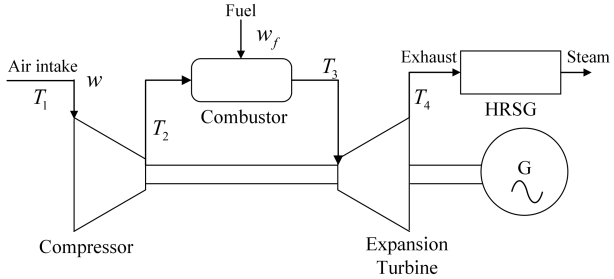

Fig. 1. A typical CHP unit with a single-shaft GT.

A. Gas Turbine Thermodynamics

In essence, all GTs are based on the Brayton cycle. Referring to the temperature-entropy diagram of the Brayton cycle in [12], it is assumed that an ideal isentropic process occurs in both the compressor and the ET. Hence, we define

$$x_c := \left(PR_n \cdot w_{pu}\right)^{\frac{\gamma_c - 1}{\gamma_c}} \tag{1}$$

$$x_h := \left(PR_n \cdot w_{pu}\right)^{\frac{\gamma_h - 1}{\gamma_h}} \tag{2}$$

where PR_n is the nominal compressor pressure ratio, and w_{pu} is the airflow rate (w) in per unit (pu). γ_c and γ_h are the cold-end and hot-end ratios of specific heats, respectively.

An irreversible adiabatic process is assumed in the compressor, so the compressor discharge temperature T_2 (K) can be calculated as:

$$T_2 = T_1\left(\frac{x_c - 1}{\eta_c} + 1\right) \tag{3}$$

where T_1 (K) is the ambient temperature and η_c is the compressor efficiency.

Likewise, the ET exhaust temperature T_4 (K) is derived as:

$$T_4 = T_3\left[1 - \left(1 - \frac{1}{x_h}\right)\eta_t\right] \tag{4}$$

where T_3 (K) is the ET inlet temperature, and η_t is the ET efficiency.

Assuming an isobar process in the combustor and considering the heat absorption rate (kJ/s) lead to

$$T_3 = T_2 + \eta_{comb}\frac{H}{C_{ph}} \cdot \frac{w_{fn}}{w_n} \cdot \frac{w_{f,pu}}{w_{pu}} \tag{5}$$

where H is the lower heating value of the fuel, and η_{comb} is the combustor efficiency. w_{fn} and w_n are the nominal fuel flow and airflow rates (kg/s), respectively. C_{ph} is the specific heat of hot-end air at constant pressure.

It is also assumed that w_f is negligible compared with w [12]. The net mechanical power produced by the GT could be calculated as

$$P_{G,pu} = \frac{P_G}{P_{Gn}} = \frac{w_{pu} \cdot w_n \cdot [C_{ph} \cdot (T_3 - T_4) - C_{pc} \cdot (T_2 - T_1)]}{P_{Gn}} \tag{6}$$

where C_{pc} is the specific heat of cold-end air at constant pressure, and P_{Gn} is the nominal gross power output (kW).

The thermal power collected by the HRSG is

$$P_{ST,pu} = K \cdot w_{pu} \cdot w_n \cdot C_{ph} \cdot T_4 \tag{7}$$

where K is a system-specific constant coefficient.

B. Control Loops

The GT-based CHP dynamic model is proposed and simulated as shown in Fig. 2. The speed governor (speed controller) is operated in standard droop mode for load sharing. It can also be in the isochronous mode to eliminate the speed deviation from the speed reference ω_{ref}.

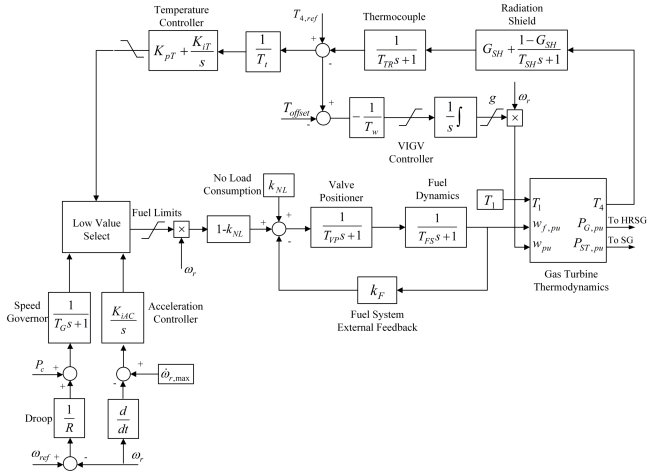

Fig. 2. Dynamic model of the GT-based CHP.

The acceleration controller limits the acceleration of the generator rotor during the start up or for a sudden loss of load. This controller becomes secondary in normal operations.

A proportional-integral (PI)-based temperature controller is employed to adjust the turbine temperature T_4 by reducing the fuel flow. If the measured T_4 exceeds the reference $T_{4,ref}$, the controller will come off the maximum limit and integrate down such that its output starts to act through the low value select block, whose output is $w_{f,pu}$.

In practice, the position g of variable inlet guide vanes (VIGVs) at the front of the compressor should be controlled to regulate the airflow drawn into the compressor when the GT is at part load or during start up. This way, T_4 can be maintained at an adequate level that benefits the downstream HRSG. In

Authorized licensed use limited to: Stevens Institute of Technology. Downloaded on February 12,2022 at 16:15:33 UTC from IEEE Xplore. Restrictions apply.

this dynamic model, T_4 is kept lower than $T_{4,ref}$ by considering an offset, e.g. 1% of the rated value. The VIGV controller modulates g, which in turn changes w_{pu} along with the rotor speed ω_r.

The no-load consumption k_{NL} ensures satisfaction of the minimum fuel requirement for self-sustaining combustion, which is crucial for compressor operation. Also, the valve positioner and fuel system dynamics are approximated as first-order transfer functions. $k_F = 0$ if the GT operates on gas fuels.

III. PV-VSG Control Scheme

Fig. 3 illustrates the topology and two-stage control diagram of the proposed PV-VSG. The front-end dc-dc boost converter is controlled to mimic the prime mover of a conventional SG, while the rear-end dc-ac inverter is controlled to mimic the SG. In the following subsections, the control modules relevant to the two stages are elaborated respectively.

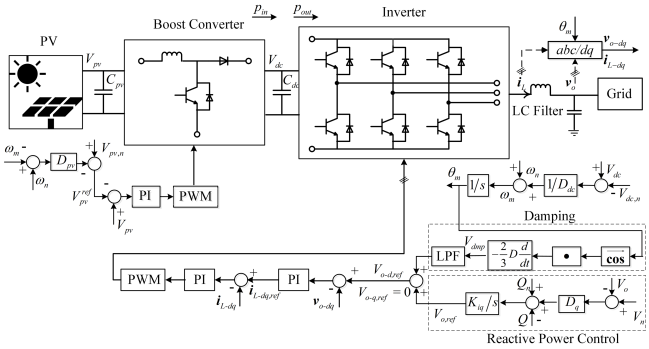

Fig. 3. Topology and control diagram of the PV-VSG.

A. Front-End Control

To avoid over-modulation and instability, the PV is operated on the right side of the MPP based on a power-voltage characteristic curve estimated directly via the measured solar irradiance and PV cell temperature [13]. Thus, a droop equation is introduced:

$$V_{pv}^{ref} = V_{pv,n} - D_{pv}(\omega_n - \omega_m) \quad (8)$$

where $V_{pv,n}$ matches the desired active power reserve to provide prime mover response, and D_{pv} is the droop coefficient. They are determined from the estimated characteristic curve. D_{pv} and $V_{pv,n}$ can also be periodically updated to keep track of the real-time operating conditions. ω_n is the nominal angular frequency, and ω_m is the virtual angular frequency generated in the rear end. A PI controller is designed with a large time constant to mimic the slow response of a prime mover. The duty cycle of the boost converter is adjusted via the PI controller so that V_{pv} closely tracks V_{pv}^{ref}. This negative feedback mechanism automatically balances the load if the available solar power is enough for active power reserve.

B. Rear-End Control

An analogy can be made between the SG rotor and the dc-link capacitor C_{dc} of the inverter using the swing equation:

$$p_{in} - p_{out} = J\omega_m\dot{\omega}_m = C_{dc}V_{dc}\dot{V}_{dc} \quad (9)$$

where J is the combined moment of inertia of SG and prime mover. C_{dc} is used to emulate the inertia. Therefore, p_{in} flowing in the direction of C_{dc} is equivalent to the mechanical power from the prime mover, and p_{out} is equivalent to the electromagnetic power across the SG air gap.

A linear mapping is adopted between the dc-link voltage V_{dc} and ω_m:

$$\omega_m = \omega_n + \frac{1}{D_{dc}}(V_{dc} - V_{dc,n}) \quad (10)$$

where $V_{dc,n}$ is the nominal dc-link voltage, and D_{dc} is the droop coefficient. It was proved in [10] that (10) along with (9) can lead to $J = D_{dc}\frac{V_{dc,n}}{\omega_n}C_{dc}$, enabling proper selection of D_{dc}.

The reactive power controller is similar to the automatic voltage regulator (AVR) plus a reactive power-voltage droop controller. The reference output voltage magnitude is obtained by integration:

$$V_{o,ref} = K_{iq}\int\left[Q_n + D_q(V_n - V_o) - Q\right]dt \quad (11)$$

where Q and V_o are the measured/calculated output reactive power and the output voltage magnitude at the LC filter. Q_n and V_n are their nominal values; D_q is the droop coefficient.

In fact, there should also be a damping power term in Eq. (9) to model the effect of SG damper windings. This paper adopts the damping method proposed in [14], since it can flexibly improve the damping of responses without compromising the desired inertia response. Define $\overrightarrow{\mathbf{sin}}(\theta) := \left[\sin(\theta) \quad \sin\left(\theta - \frac{2\pi}{3}\right) \quad \sin\left(\theta + \frac{2\pi}{3}\right)\right]$ and $\overrightarrow{\mathbf{cos}}(\theta) := \left[\cos(\theta) \quad \cos\left(\theta - \frac{2\pi}{3}\right) \quad \cos\left(\theta + \frac{2\pi}{3}\right)\right]$. Assuming the actual output voltage $\boldsymbol{v}_o = V_o\,\overrightarrow{\mathbf{sin}}(\theta_o)$, the derivative of the inner product readily yields the difference between ω_o and ω_m:

$$\frac{d}{dt}(\langle \boldsymbol{v}_o, \overrightarrow{\mathbf{cos}}(\theta_m)\rangle) = \frac{3}{2}V_o(\omega_o - \omega_m)cos(\theta_o - \theta_m) \quad (12)$$

hence, the damping term $V_{dmp} = -\frac{2}{3}D\frac{d}{dt}(\langle \boldsymbol{v}_o, \overrightarrow{\mathbf{cos}}(\theta_m)\rangle)$ is added to $V_{o,ref}$ to generate the modified reference voltage magnitude $V_{o-d,ref}$; D is the damping coefficient. A low-pass filter (LPF) is employed because the derivative can amplify high-frequency noises. The inverter reference voltage is generated via two cascaded PI controllers working in the synchronous d-q reference frame.

It is noteworthy that the proposed PV-VSG without ESSs may be limited in mitigating large SI fluctuations, especially when it operates alone and the available solar power suddenly becomes insufficient. Thus, coordinated control with other DERs is necessary to improve power quality. In the case of severe power deficits, UFLS schemes can be further pursued to maintain the frequency.

IV. Simulation of the Coordinated Control Between the Two Systems in the Campus Microgrid

To validate the GT-based CHP and PV-VSG models and demonstrate their coordinated control in an islanded campus microgrid, numerical simulations of a prototype campus microgrid as shown in Fig. 4 are implemented in MATLAB/Simulink. During a utility power outage, the campus microgrid

Authorized licensed use limited to: Stevens Institute of Technology. Downloaded on February 12,2022 at 16:15:33 UTC from IEEE Xplore. Restrictions apply.

will operate in the islanded mode, i.e., the static switch at Bus 1 remains opened. The capacitor bank (CB) is activated for reactive power support. During school days, the loads at Bus 4 and Bus 5 are identified as critical, while the other loads are noncritical ones. The 5-MVA Centaur 40 CHP model contains a salient-pole SG fitted with the generic IEEE DC1A exciter. Averaged models of the boost converter and the inverter are employed in the PV-VSG model for simulation speedup. The detailed control and system parameters are given in [15].

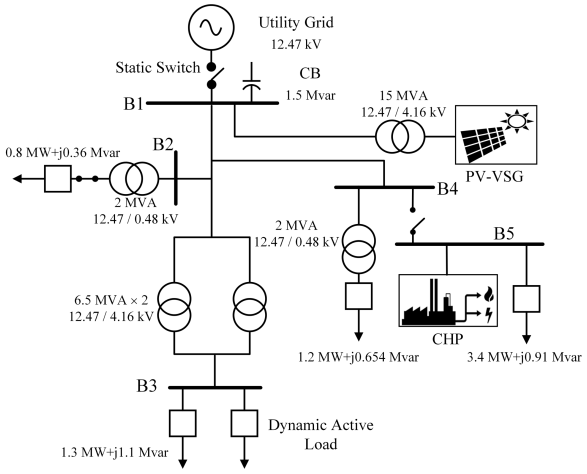

Fig. 4. Single-line diagram of the campus microgrid system.

The dynamic active load at Bus 3 is modeled to test the transient performance of the proposed PV-VSG under different loading conditions. Specifically, the dynamic active load experiences a step increase from 0 to 1.2 MW at t = 10.2 s and then a step decrease to 0.8 MW at t = 18.7 s. To further explore the effect of solar irradiance (SI) on the PV-VSG operation, a varying SI shown in Fig. 5 is used throughout the simulation.

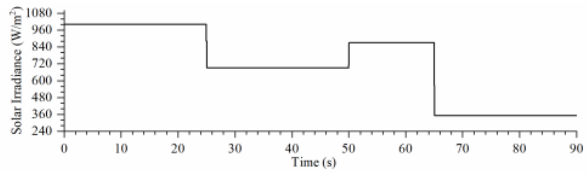

Fig. 5. Solar irradiance curve.

In order to illustrate the coordinated control of the CHP and PV-VSG, the simulation scenario is designed such that the CHP unit only supplies the local load at Bus 5 initially and can enter the hot standby mode once dispatched. The rest of the campus is served by the PV farm with the assumption that the available solar power is initially adequate to provide active power reserve. However, since the grid frequency may drop due to plunged SI or increased campus loads, UFLS should be in place to prevent the frequency from falling below the minimum permissible value, e.g., 59.3 Hz. When the frequency stabilizes after some transients, the CHP unit will start to synchronize to deliver reliable power and enhance system inertia. It should be noted the design of a UFLS scheme is system-specific and beyond the scope of this paper. For simplification, we set the UFLS such that the load at Bus 2 will be shed when the system frequency reaches 59.7 Hz, and the dynamic active load will be shed once the frequency drops below 59.6 Hz. Other loads are shed in further steps when lower frequency thresholds are met. And this relay setting is consistent before and after CHP synchronization. The ambient temperature is assumed to be 27.5 °C, and $V_{dc,n}$ is 10 kV. $V_{pv,n}$ is initially set as 5847 V, resulting in an active power reserve of around 5 MW. The total simulation time is 90 s with a time step of 50 μs.

The dc-link voltage of PV-VSG and the angular frequencies of both DERs during the simulation are presented in Fig. 6. As shown in Fig. 6, with a constant SI in the first 25 seconds, the PV-VSG solely responds to the change in loads with a varied V_{dc}, which relates to a constantly identical waveform of ω_m due to the introduced linear transformation. It is also observed that a change in SI leads to a variation in V_{dc} and ω_m, e.g., at the transient right after t = 25 s. However, the frequency does not change rapidly due to the inertia emulated by the capacitor. The CHP unit is called upon as hot standby at t = 20 s. Pre-synchronization is initiated at t = 27.93 s when the system frequency stabilizes at 59.75 Hz after the SI decreases for the first time. CHP synchronizes to the rest of the grid at t = 31.06 s for load sharing. Meanwhile, the governor speed reference ω_{ref} is adjusted from 1.008 pu to 1.014 pu and remains fixed afterwards. Owing to the CHP's participation in frequency regulation, the grid frequency recovers and settles at 59.928 Hz at t = 35.51 s. As the SI goes up at t = 50 s, the PV power is adequate to supply the loads such that the dc-link capacitor is recharged, thus increasing both ω_m and V_{dc}. At t = 65 s, SI plummets from 870 to 350 W/m^2. The UFLS protective relays are automatically triggered at t = 65.37 s and t = 65.69 s to shed the load at Bus 2 and the dynamic active load, respectively. The frequency finally settles at 59.806 Hz. Fig. 7 displays the power outputs of the two DERs throughout the simulation.

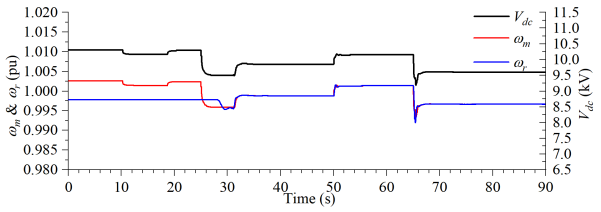

Fig. 6. CHP and PV-VSG frequency responses and PV-VSG dc-link voltage.

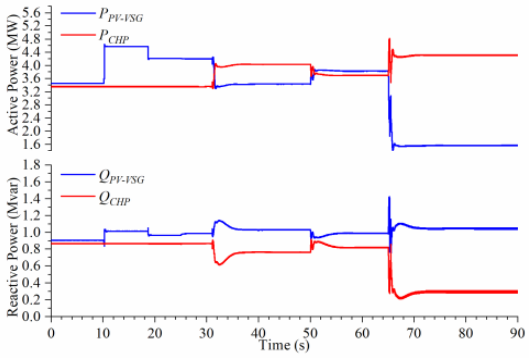

Fig. 7. Active and reactive power outputs of CHP and PV-VSG.

Authorized licensed use limited to: Stevens Institute of Technology. Downloaded on February 12,2022 at 16:15:33 UTC from IEEE Xplore. Restrictions apply.

It is clear that, before the CHP is synchronized, the PV-VSG is able to achieve automatic load balancing despite variations in the SI. This capability is ensured by sufficient active power reserve. After the CHP unit is synchronized to the microgrid, it begins to pick up part of the loads. Interestingly, the active power shared by the CHP and PV systems are not in a fixed proportion at all times but affected by the varying SI. After the SI plunges at t = 65 s, the CHP unit takes over too much active power and almost reaches its apparent power rating. Consequently, the reactive power capability of the CHP unit becomes very limited. It is also worth noting that the CHP unit alone cannot serve the entire electrical load of the campus once the sun stops shining. Hence, uprating the existing CHP unit or installing additional CHP units would be favorable to the stable and safe operation of the campus microgrid.

The variables related to the thermodynamic equations of the CHP's gas turbine are illustrated in Fig. 8.

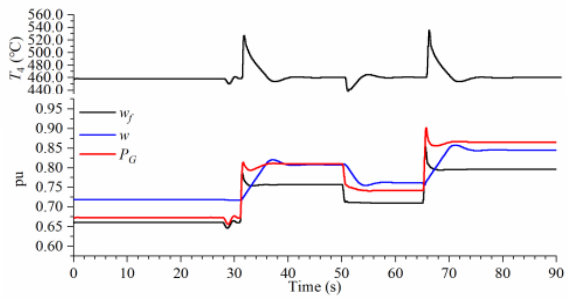

Fig. 8. Illustration of the variables in the GT thermodynamic equations.

Prior to synchronization, the GT exhaust temperature is maintained close to the reference value 465 °C, albeit at part load. This is because the VIGV controller is in action, which regulates w to a relatively low level. Once the CHP is synchronized, the fuel flow rate rises so as to provide a higher mechanical power output. As T_4 surpasses the reference, w is controlled to reach a higher level so that T_4 is brought back near the reference again. It is also observed from Fig. 8 that the temperature controller also acts by decreasing w_f, which is evidenced after the instants t = 31.06 s and t = 65.69 s. However, the VIGV control has a slower response than the fuel flow rate control. Besides, Fig. 8 shows that the mechanical power output P_G varies almost linearly with w_f, which checks with the aforementioned GT thermodynamic equations.

It has also been verified that the voltage magnitudes at all buses are maintained within the typical permissible bounds from 0.95 to 1.05 pu as shown in Fig. 9, when the campus microgrid is in islanded mode.

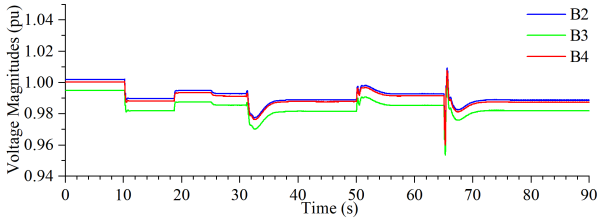

Fig. 9. Voltage magnitudes at various buses.

V. Conclusions

In this paper, a campus microgrid coordinately supplied and controlled by the CHP and PV systems in islanded mode is modeled with high precision. A double-stage PV-VSG control scheme is proposed to study the integration of a 10-MW PV farm. This method utilizes the dc-link capacitor for inertia emulation and demonstrates satisfactory transient performance under varying operating conditions. Moreover, the feasibility of the coordinated control between the two systems for stable operation has been corroborated in the numerical simulations. However, the proposed PV-VSG operates with a variation in the dc-link voltage and operating alone needs the supplement of UFLS in the case of plunging SI. In the future, we plan to integrate an ESS with the dc-link capacitor to further improve inertia support and transient stability. Electricity and gas co-optimization will also be considered in the campus microgrid for enhanced campus energy system economic operation.

References

[1] W. I. Rowen, "Simplified mathematical representations of single shaft gas turbines in mechanical drive service," presented at *the Int. Gas Turbine and Aeroengine Congr. and Expo*., Cologne, Germany, 1992.

[2] Task Force on Turbine-Governor Modeling, "Dynamic models for turbine-governors in power system studies," *IEEE PES Technical Report*, Jan. 2013.

[3] N. Hadroug *et al*, "Heavy duty gas turbine monitoring based on adaptive neuro-fuzzy inference system: speed and exhaust temperature control," *Mathematics-in-Industry Case Studies*, 8, 8, 2017.

[4] T. Sun, J. Lu, Z. Li, D. Lubkeman, and N. Lu, "Modeling combined heat and power systems for microgrid applications," *IEEE Transactions on Smart Grid*, vol. 9, no. 5, pp. 4172-4180, 2018.

[5] R. H. Lasseter, Z. Chen, and D. Pattabiraman, "Grid-forming inverters: A critical asset for the power grid," *IEEE J. Emerg. Sel. Topics Power Electron.*, vol. 8, no. 2, pp. 925-935, June 2020.

[6] M. Mao, C. Qian, and Y. Ding, "Decentralized coordination power control for islanding microgrid based on PV/BES-VSG," *CPSS Trans. on Power Electron. and Appl.*, vol. 3, no. 1, pp. 14-24, March 2018.

[7] X. Yan, X. Zhang, *et al*., "Research on distributed PV storage virtual synchronous generator system and its static frequency characteristic analysis," *Appl. Sci.* 2018, *8*, 532.

[8] A. Hoke, M. Shirazi, *et. al*, "Rapid active power control of photovoltaic systems for grid frequency support," *IEEE Trans. Emerg. Sel. Topics Power Electron.,* vol. 5, no. 3, pp. 1154-1163, Feb. 2017.

[9] X. Zhang, Q. Gao, *et al.*, "Active power reserve photovoltaic virtual synchronization control technology," *Chinese J. of Electr. Eng.*, vol. 6, no. 2, pp. 1-6, June 2020.

[10] S. A. Khajehoddin, M. Karimi-Ghartemani, and M. Ebrahimi, "Grid supporting inverters with improved dynamics," *IEEE Transactions on Industrial Electronics*, vol. 66, no. 5, pp. 3655-3667, May 2019.

[11] X. Yan, J. Li, *et al*., "Adaptive-MPPT-based control of improved photovoltaic virtual synchronous generators," *Energies* 2018, *11*, 1834.

[12] M. R. B. Tavakoli, B. Vahidi, and W. Gawlik, "An educational guide to extract the parameters of heavy duty gas turbines model in dynamic studies based on operational data," *IEEE Transactions on Power Systems*, vol. 24, no. 3, pp. 1366-1374, Aug. 2009.

[13] J. Bai *et al.*, "Development of a new compound method to extract the five parameters of PV modules," *Energy Conversion and Management*, vol. 79, pp. 294-303, March 2014.

[14] M. Ebrahimi, S. A. Khajehoddin, and M. Karimi-Ghartemani, "An improved damping method for virtual synchronous machines," *IEEE Trans Sustain Energy*, vol. 10, no. 3, pp. 1491-1500, July 2019.

[15] Data file for the Simplified Campus Microgrid. [Online]. Available: https://github.com/jimzhang90/Test-System-Data.

Authorized licensed use limited to: Stevens Institute of Technology. Downloaded on February 12,2022 at 16:15:33 UTC from IEEE Xplore. Restrictions apply.